A Newton-Type Current Injection Model of UPFC for Studying Low-Frequency Oscillations

Kwang M. Son, *Member, IEEE,* and Robert H. Lasseter, *Fellow, IEEE*

***Abstract*—This paper presents a Newton-type current injection model of the unified power flow controller (UPFC) for studying the effect of the UPFC on the low-frequency oscillations. Since the proposed model is a Newton-type one, it is conceptually simple and gives fast convergence characteristics. The model is applied to an inter-area power oscillation damping regulator design of a sample two-area power system. The damping achievable by the UPFC equipped with damping regulator is investigated in both frequency and time domains using the proposed model. The case study results in this paper show that the proposed model is efficient for studying the effects of the UPFC on the inter-area oscillations.**

***Index Terms*—Flexible ac transmission systems (FACTS), power system oscillation damping, unified power flow controller (UPFC).**

I. Introduction

FLEXIBLE ac transmission system (FACTS) devices give more flexibility of control for secure and economic operation of power systems [1]. Among FACTS devices, the unified power flow controller (UPFC) is emerging as a promising solution for improving power system characteristics for its high degree of controllability of many power system variables [2].

Studies on the dynamic modeling, simulation, and control of UPFC are currently undertaken [3]–[9]. [3] proposed a detailed dynamic modeling of UPFC based on switching functions with time domain simulations using EMTP.

In the power frequency range, UPFC variables such as injected voltage and currents are expressed as phasors [4]–[8]. Difficulties of modeling UPFC in the conventional dynamic simulation programs arise from the fact that the injected voltage by the series inverter is superimposed on the shunt inverter side voltage. The resulting voltage of the series inverter side depends on the phase of the shunt inverter side voltage that is also affected by the series injected voltage. Therefore, the relations are implicit and nonlinear, which should be solved iteratively at every time step of dynamic simulation.

In [4], a power injection model was used to study the effect of UPFC for improving damping of oscillations with an energy function-based control strategy. The power injection model is derived from the power balance equations at the UPFC-network interface nodes. The power flow Jacobian is slightly expanded and the power flow equations are solved at every time step.

Manuscript received November 25, 2002. This work was supported in part by a postdoctoral fellowship program from Korea Science and Engineering Foundation (KOSEF).

K. M. Son is with the Department of Electrical Engineering, Dong-Eui University, Pusan, 614-714, Korea (e-mail: kmson@dongeui.ac.kr).

R. H. Lasseter is with the Department of Electrical and Computer Engineering, University of Wisconsin-Madison, Madison, WI 53706 USA (e-mail: lasseter@engr.wisc.edu).

Digital Object Identifier 10.1109/TPWRD.2003.822543

Since many dynamic simulation programs adopt current balance equations for solving network equations, it should also be taken into account modeling UPFC as current injections and finding the interface variables satisfying the interface conditions.

There are several approaches in the current injection model [5], [7], [8]. In [5], an iterative scheme, which finds UPFC injection currents satisfying UPFC-network interface conditions, has been developed. The external network is represented by its Thevnin equivalent. The injection currents are successively updated using the above relations until convergence is reached. In [7], the bus admittance matrix is reduced to the generator internal buses and the currents injected by the UPFC are substituted into the network equations. As a result, a two-dimensional complex vector equation is solved at every step until the UPFC-network interface node voltages converge. The dc link capacitor dynamics are also included in the proposed model. In [8], A linearized Heffron–Phillips model of a power system installed with a UPFC is proposed and the effect of the dc voltage regulator on the power oscillation damping is investigated. [8], however, does not explicitly discuss the algorithm of nonlinear time domain simulations.

This paper proposes a current injection model of UPFC to study the effect of UPFC on the power system low-frequency oscillations. Since the models of [5] and [7] adopt fixed-point iteration schemes, they guarantee only linear convergence and the iteration processes are not so intuitive. The main contribution of this paper is the derivation of the Newton-type iteration formulation based on the current balance equations. Since the proposed model is a Newton type, it is conceptually simple and has quadratic convergence characteristics. The derived model can be applied to any type of generator models, networks and loads. When all loads have constant impedance characteristics, the resulting equations become similar to the iteration formula by [7] with the exception that the Newton iteration is applied to the proposed equation.

The model is applied to the controller design for damping inter-area oscillations in the sample two-area power system model. The characteristics of the damping controller are investigated both in the time and frequency domains. Case study results show that simulations using the proposed model converge rapidly.

II. UPFC Modeling

Appropriate modeling of the UPFC depends on the range of frequency of concern. The model required for studying low-frequency oscillations should faithfully exhibit phenomena of 0.1–2 Hz.

It has been shown that dc voltage regulator can have a negative effect on damping of the transient caused by the fault [8]. The fluctuation of the dc link voltage stems from the disability of the shunt inverter to supply the energy needed to inject to the system through the series inverter [10]. In that case, the energy of the dc link capacitor is used to supply the needed energy and as a result the dc link voltage regulator's action dominates.

It has been shown in [7] that dc capacitor voltage fluctuation during transient is less than 1.5% of the rated voltage for the studied case. And, in real situations, the magnitude of the series injected voltage to modulate the real power for damping control is limited within a small range in order not to excite nonlinear dynamics. So it does not cause much error to assume that the shunt inverter can supply the oscillations of the real power and the dc capacitor voltage is stiff especially for the above mentioned frequency range. The resulting UPFC model under consideration is shown in Fig. 1(a), as in [3].

The series injected voltage can be converted to its equivalent injection current sources as shown in the Fig. 1(b). The current injection model can be easily adopted for the conventional power system simulation programs, except one difficulty that the injected currents are dependent on the UPFC side voltage $\mathbf{V}_{N-1}$, which implies that the current injection of the UPFC should be solved using an iterative technique.

III. Conventional Dynamic Simulations [11], [12]

Among various dynamic simulation methods, many dynamic simulation programs adopt the current-balance form for solving network equations of the system. The power system dynamic model can be written as a set of differential equations (1) and a set of algebraic equations (2) as a vector form

$$\dot{\mathbf{x}} = \mathbf{f}(\mathbf{x}, \mathbf{V}) \tag{1}$$

$$\mathbf{I}(\mathbf{x}, \mathbf{V}) = \mathbf{Y}\mathbf{V} \tag{2}$$

where $\mathbf{I}$ and $\mathbf{V}$ are complex injection currents and voltage vectors of dimension n, respectively, and $\mathbf{x}$ is a state variable vector of dimension m. The number n is equal to the number of nodes of the system and the number m depends on the number and the type of the dynamic models used. Nonlinear static loads are treated as injection currents dependent on their own bus voltages as shown in (2). So, algebraic equations are, in general, implicit and nonlinear. Equation (2) can be re-written as

$$\mathbf{F} = \mathbf{I}(\mathbf{x}, \mathbf{V}) - \mathbf{Y}\mathbf{V} = \mathbf{0}. \tag{3}$$

Dividing (3) into real and imaginary parts and then calculating $2n$-by-$2n$ Jacobian gives a Newton iteration formula

$$\begin{bmatrix} F_R \\ F_I \end{bmatrix} = \begin{bmatrix} \frac{\partial F_R}{\partial V} & \frac{\partial F_R}{\partial \theta} \\ \frac{\partial F_I}{\partial V} & \frac{\partial F_I}{\partial \theta} \end{bmatrix} \begin{bmatrix} \Delta V \\ \Delta \theta \end{bmatrix} = \mathbf{J} \begin{bmatrix} \Delta V \\ \Delta \theta \end{bmatrix} \tag{4}$$

where the subscripts R and I indicate real and imaginary part, respectively. In the explicit integration approach, (1) is used to update the state variables $\mathbf{x}$ and then the algebraic variables in (2) are solved by the Newton formula given by (4), at every step.

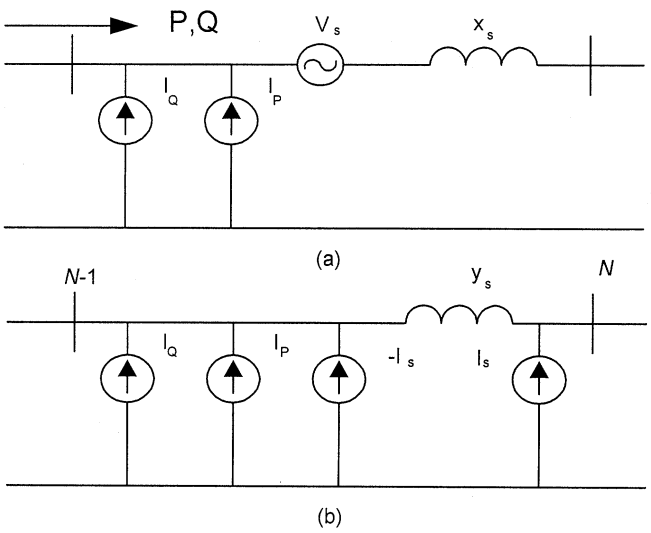

Fig. 1. (a) UPFC model and (b) its equivalent current injection model.

IV. The Proposed Model

A. UPFC Augments the Conventional Jacobian

Since the state vector $\mathbf{x}$ is updated before algebraic variables are calculated at every step in the explicit integration approach, the dependence on $\mathbf{x}$ in (3) can be suppressed when solving algebraic variables. It is assumed that UPFC is installed in the middle of transmission line. In case a UPFC is installed, the number of nodes becomes $N = n + 2$ and the conventional algebraic equations (3) become

$$\mathbf{F}_A = \begin{bmatrix} \mathbf{I}(\mathbf{V}) \\ \mathbf{I}^u(\mathbf{V}^u) \end{bmatrix} - \begin{bmatrix} \mathbf{Y} & \mathbf{Y}^m \\ \mathbf{Y}^n & \mathbf{Y}^u \end{bmatrix} \begin{bmatrix} \mathbf{V} \\ \mathbf{V}^u \end{bmatrix} \triangleq \mathbf{I}_A(\mathbf{V}_A) - \mathbf{Y}_A\mathbf{V}_A = \mathbf{0} \tag{5}$$

where $\mathbf{I}$ and $\mathbf{V}$ are conventional n dimensional complex injection current and voltage vectors in (2), respectively. In (5), $\mathbf{I}^u$ and $\mathbf{V}^u$ are 2- D complex UPFC injection current and voltage vectors with $\boldsymbol{\theta}^u$ being the phase angle of the corresponding voltage as follows:

$$\mathbf{I}^u = \begin{bmatrix} \mathbf{I}_1^u \\ \mathbf{I}_2^u \end{bmatrix}, \quad \mathbf{V}^u = \begin{bmatrix} \mathbf{V}_1^u \\ \mathbf{V}_2^u \end{bmatrix} = \begin{bmatrix} V_1^u \angle \theta_1^u \\ V_2^u \angle \theta_2^u \end{bmatrix} \tag{6}$$

where subscript 1 corresponds to the shunt inverter side node ($N - 1$ in Fig. 1) and the subscript 2 to the series inverter or line side node (N in Fig. 1), respectively. The subscript A in (5) implies the augmented quantities. The submatrix $\mathbf{Y}$ is an n-by-n conventional bus admittance matrix including network and generator stator transient impedances as in (2), and $\mathbf{Y}^m$ and $\mathbf{Y}^n$ are mutual admittance matrices between the UPFC nodes and the network. $\mathbf{Y}^u$ relates the UPFC inverter side node and the line side node, respectively.

Decomposing (5) into real and imaginary parts and then calculating the partial derivatives of the $2N$ equations with respect to $2N$ unknown variables gives a Newton formula with a $2N$-by-$2N$ Jacobian as

$$\begin{bmatrix} \Delta F_R \\ \Delta F_I \\ \Delta F_R^u \\ \Delta F_I^u \end{bmatrix} = \begin{bmatrix} \mathbf{J} & \mathbf{J}^m \\ \mathbf{J}^n & \mathbf{J}^u \end{bmatrix} \begin{bmatrix} \Delta V \\ \Delta\theta \\ \Delta V^u \\ \Delta\theta^u \end{bmatrix} \text{ or } \Delta F_A = \mathbf{J}_A \Delta V_A \quad (7)$$

where $\mathbf{J}$ is the conventional $2n$-by-$2n$ Jacobian corresponding to (4) and $\mathbf{J}^m$, $\mathbf{J}^n$ and $\mathbf{J}^u$ are augmented parts due to UPFC.

B. Elements of $\mathbf{J}^m$ and $\mathbf{J}^n$

Equation (8) shows the blocks of $\mathbf{J}^m$ which are all n-by-2 submatrices

$$\mathbf{J}^m = \begin{bmatrix} \frac{\partial F_R}{\partial V^u} & \frac{\partial F_R}{\partial \theta^u} \\ \frac{\partial F_I}{\partial V^u} & \frac{\partial F_I}{\partial \theta^u} \end{bmatrix}. \quad (8)$$

In order to derive the elements of $\mathbf{J}^m$, (5) can be rewritten as two complex valued vector functions with dimensions of n and 2, respectively, in the following form:

$$\mathbf{F} = \mathbf{I}(\mathbf{V}) - \mathbf{Y}\mathbf{V} - \mathbf{Y}^m\mathbf{V}^u = \mathbf{0} \quad (9)$$

$$\mathbf{F}^u = \mathbf{I}^u(\mathbf{V}^u) - \mathbf{Y}^n\mathbf{V} - \mathbf{Y}^u\mathbf{V}^u = \mathbf{0}. \quad (10)$$

Taking partial derivatives of (9) with respect to the UPFC voltage magnitude and phase angle gives expressions for the elements of $\mathbf{J}^m$. Since only the third term in (9) depends on $\mathbf{V}^u$, we have only to consider $-\mathbf{Y}^m\mathbf{V}^u$ in calculating partial derivatives. Let the elements of the admittance matrix $\mathbf{Y}^m$ and the UPFC voltage be defined for $i = 1, 2, \ldots, n$ and $k = 1, 2$ as follows:

$$\mathbf{Y}_{ik}^m = Y_{ik}^m \exp(j\phi_{ik}^m), \quad \mathbf{V}_k^u = V_k^u \exp(j\theta_k^u). \quad (11)$$

The elements of the Jacobian can be obtained as

$$\frac{\partial \mathbf{F}_i}{\partial V_k^u} = -Y_{ik}^m \exp\left(j\left(\phi_{ik}^m + \theta_k^u\right)\right) \quad (12)$$

$$\frac{\partial \mathbf{F}_i}{\partial \theta_k^u} = -jY_{ik}^m V_k^u \exp\left(j\left(\phi_{ik}^m + \theta_k^u\right)\right). \quad (13)$$

Taking real and imaginary part of (12) and (13) gives the final expression for each element of $\mathbf{J}^m$

$$\frac{\partial F_{Ri}}{\partial V_k^u} = -Y_{ik}^m \cos\left(\phi_{ik}^m + \theta_k^u\right) \quad (14)$$

$$\frac{\partial F_{Ii}}{\partial V_k^u} = -Y_{ik}^m \sin\left(\phi_{ik}^m + \theta_k^u\right) \quad (15)$$

$$\frac{\partial F_{Ri}}{\partial \theta_k^u} = Y_{ik}^m V_k^u \sin\left(\phi_{ik}^m + \theta_k^u\right) \quad (16)$$

$$\frac{\partial F_{Ii}}{\partial \theta_k^u} = -Y_{ik}^m V_k^u \cos\left(\phi_{ik}^m + \theta_k^u\right). \quad (17)$$

The elements of $\mathbf{J}^n$ can be derived in the same way except taking partial derivatives of (10) with respect to $\mathbf{V}$. In this case, since only the second term depends on $\mathbf{V}$, we have only to consider $-\mathbf{Y}^n\mathbf{V}$.

C. Elements of $\mathbf{J}^u$

In (10), the term $\mathbf{I}^u(\mathbf{V}^u)$ accounts for the dependence of the UPFC injection current on its own voltages, which makes it difficult to incorporate UPFC directly in the conventional dynamic simulation algorithm.

In order to obtain the elements of $\mathbf{J}^u$, we need to investigate a more detailed expression of UPFC injection current. From the equivalent current injection model, as in Fig. 1, the injection current at the UPFC node ($N-1$ and N) can be expressed as

$$\mathbf{I}^u(\mathbf{V}^u) = \begin{bmatrix} \mathbf{I}_P(\mathbf{V}^u) + \mathbf{I}_Q - \mathbf{I}_S(\theta^u) \\ \mathbf{I}_S(\theta^u) \end{bmatrix}. \quad (18)$$

The shunt inverter injection currents decomposed into two parts. $\mathbf{I}_P$ is in phase with the node voltage so to supply the real power that the series inverter needs. $\mathbf{I}_Q$ is the reactive current component independently controlled by the shunt converter. The series injected voltage has been converted to its equivalent current source $\mathbf{I}_S$ in (18).

The magnitude and phase of the series injected voltage, $\mathbf{V}_S$, can be independently controlled by the control system. However, since the series injected voltage is superimposed on the shunt inverter side voltage, the phase of the injection current should depend on the phase of the shunt inverter side voltage as

$$\mathbf{I}_S = \frac{\mathbf{V}_S \exp j\theta_1^u}{jx_S}, \quad \mathbf{V}_S = V_S \exp j\theta_S \quad (19)$$

where θ_1 denotes the phase angle of the inverter side voltage.

In the shunt inverter $\mathbf{I}_P$ is determined from the real power that is injected by the series inverter. From the real power conservation, neglecting losses of the inverter, we can get

$$\mathbf{I}_P = -\frac{\mathrm{Re}[\mathbf{V}_S\mathbf{I}_S^*]}{\mathbf{V}_1^{u^*}}. \quad (20)$$

The reactive injection current by the shunt inverter is quadrature phase with the shunt inverter side voltage in order to inject the reactive power into the power system

$$\mathbf{I}_Q = I_Q \exp j\left(\theta_1^u - \frac{\pi}{2}\right). \quad (21)$$

Using the relations given by (19)–(21) in (18), we can get the elements of 4-by-4 real matrix $\mathbf{J}^u$. Each submatrix shown in (22) has a dimension of 2-by-2, the elements of which are listed in Appendix A

$$\mathbf{J}^u = \begin{bmatrix} \frac{\partial F_R^u}{\partial V^u} & \frac{\partial F_R^u}{\partial \theta^u} \\ \frac{\partial F_I^u}{\partial V^u} & \frac{\partial F_I^u}{\partial \theta^u} \end{bmatrix}. \quad (22)$$

Some comments follow.

1) Although the proposed approach assumes the explicit integration as a simulation method, it can be easily extended to the case of an implicit integration method. In that case, Jacobian of the state equations is also formed and state variables are solved simultaneously with the algebraic variables.
2) The proposed method can be directly applied to the system with any number of UPFCs. For example, If one more UPFC is installed, the injection current and voltage vectors corresponding to the UPFC are added in (5) and the same procedure is applied to form a Jacobian.

D. Special Case of Constant Impedance Loads

In case all loads are constant impedance type, $\mathbf{I}$ in (5) is directly determined from the state variables of generators and excitation systems at every iteration step. Thus, when we solve the algebraic equations at every step, $\mathbf{I}$ is given as a pre-determined constant. Therefore, (5) becomes

$$\begin{bmatrix} \mathbf{I} \\ \mathbf{I}^u(\mathbf{V}^u) \end{bmatrix} = \begin{bmatrix} \mathbf{Y} & \mathbf{Y}^m \\ \mathbf{Y}^n & \mathbf{I}^u \end{bmatrix} \begin{bmatrix} \mathbf{V} \\ \mathbf{V}^u \end{bmatrix}. \tag{23}$$

Noting that only $\mathbf{I}^u$ is a function of $\mathbf{V}^u$, $\mathbf{V}$ can be expressed by $\mathbf{V}^u$ as follows:

$$\mathbf{V} = \mathbf{Y}^{-1}(\mathbf{I} - \mathbf{Y}^m\mathbf{V}^u). \tag{24}$$

Using (24) in (23), $\mathbf{I}^u$ can be expressed as

$$\mathbf{I}^u(\mathbf{V}^u) = \mathbf{Y}^n\mathbf{Y}^{-1}\mathbf{I} + (\mathbf{Y}^u - \mathbf{Y}^n\mathbf{Y}^{-1}\mathbf{Y}^m)\mathbf{V}^u \tag{25}$$

where $\mathbf{I}$ is a constant matrix and $\mathbf{V}^u$ can be solved by a Newton-type method if we set

$$\mathbf{Y}_0 = \mathbf{Y}^n\mathbf{Y}^{-1}\mathbf{I}, \quad \mathbf{Y}_R = \mathbf{Y}^u - \mathbf{Y}^n\mathbf{Y}^{-1}\mathbf{Y}^m. \tag{26}$$

Then, (25) becomes 2-D complex valued functions (27). The corresponding Jacobian is exactly the same as $\mathbf{J}^u$ shown in the Appendix except that $\mathbf{Y}^u$ is replaced by $\mathbf{Y}_R$.

$$\mathbf{I}^u(\mathbf{V}^u) - \mathbf{Y}_R\mathbf{V}^u - \mathbf{Y}_0 = \mathbf{0}. \tag{27}$$

Some comments follow.

1) In case all loads are constant impedance type, the algorithm has only to find out the solutions that satisfy the interface conditions at the UPFC node (27). Once the voltages at the UPFC are found, the voltages at the other nodes are found by (24).
2) Only the 4-by-4 matrix, $\mathbf{J}^u$, need to be calculated for each iteration step if a single UPFC is installed in the system. The dimension of the Jacobian evaluated at every iteration step depends on the number of nonlinear loads and the number of UPFCs installed.

V. Damping Controller Design

A. A Sample Power System Model

A sample system used in the case study is a simple two-area four-machine power system model in [11] (see also Fig. 2). It is assumed that a UPFC is installed in the middle of the 200 km tie-lines. All generators are fourth-order two-axis models equipped with 1st order fast exciters. The equations of the two-axis models appear in [12]. All the exciter parameters are the same as $K_A = 200\ (\text{pu})$, $T_A = 0.02\ (\text{s})$. The machine and system parameters are listed in the Appendix. All loads are assumed to be constant impedance type.

The system has one inter-area mode with very poor damping. Three operating points under consideration similar to the cases in [13] are listed in Table I. The median system is the nominal system that the damping controller is designed. The weak system is an unstable case with one tie-line out of service.

TABLE I
Operating Points Under Consideration

System	Tie Flow (MW)	# of ties	Gen/Load (MW)		Damping Ratio(%)
			Area 1	Area 2	
Stiff	4	3	1120/970	1400/1390	2.82
Median	360	3	1400/970	1400/1740	0.156
Weak	360	2	1400/970	1400/1740	−0.175

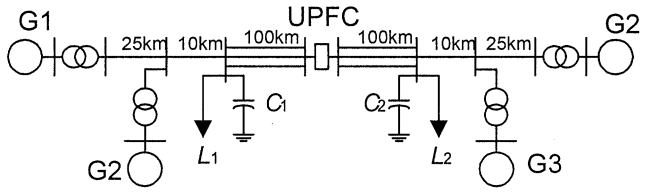

Fig. 2. A sample two-area power system model.

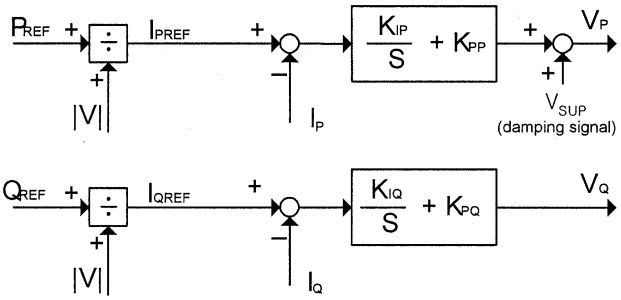

Fig. 3. The series part of the control system of UPFC.

B. Linearization Approach

In order to analyze the performance of the system with UPFC using the proposed approach, we need to linearize the system given by (1) and (5). Taking partial derivatives of (1) and (5) gives

$$\Delta\dot{\mathbf{x}} = \frac{\partial \mathbf{f}}{\partial \mathbf{x}}\Delta\mathbf{x} + \frac{\partial \mathbf{f}}{\partial V_A}\Delta V_A \tag{28}$$

$$\frac{\partial F_A}{\partial \mathbf{x}}\Delta\mathbf{x} + \frac{\partial F_A}{\partial V_A}\Delta V_A = \mathbf{0} \tag{29}$$

where V_A is defined in (7). Using the fact that $\partial F_A/\partial V_A = \mathbf{J}_A$ and substitution of (29) into (28) give

$$\Delta\dot{\mathbf{x}} = \left[\frac{\partial \mathbf{f}}{\partial \mathbf{x}} - \frac{\partial \mathbf{f}}{\partial V_A}\mathbf{J}_A^{-1}\frac{\partial F_A}{\partial \mathbf{x}}\right]\Delta\mathbf{x} \triangleq \mathbf{A}\Delta\mathbf{x}. \tag{30}$$

Equation (30) shows the relations of the augmented Jacobian and the state matrix.

C. UPFC Control System

Fig. 3 shows the structure of the control system of the series part of the UPFC as described in [14]. PI-type regulators control the series injected voltage. In order to focus on the series part for its effectiveness for damping, we consider only controlling series injected voltage for damping control. It is assumed that the control system has a supplementary input as shown in Fig. 3. The series injected voltage $\mathbf{V}_S$ is decomposed into the

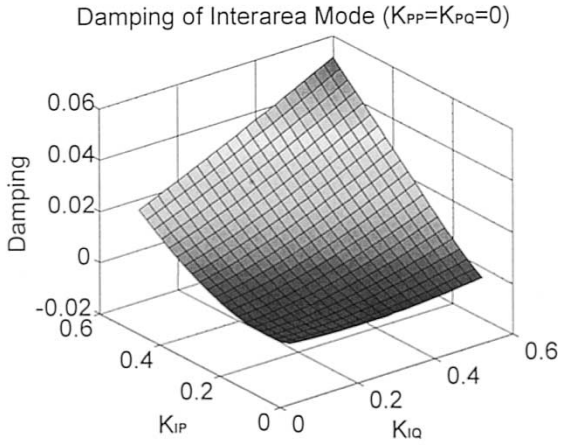

Fig. 4. Damping of inter-area mode with changing K_{IP} and K_{IQ}.

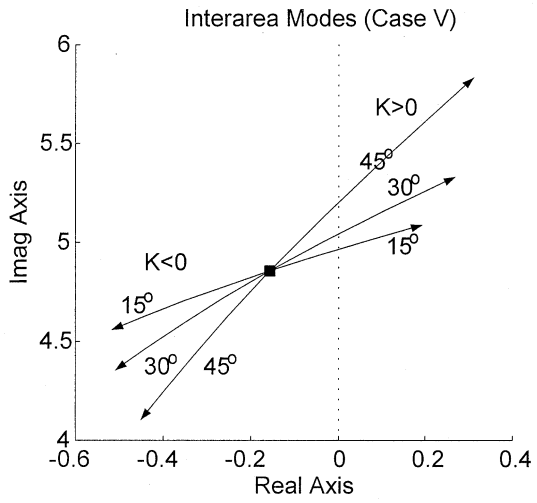

Fig. 5. Loci of inter-area mode for various phase lead angle and gain.

in-phase component V_P and quadrature-phase component V_Q in the UPFC control system as shown in Fig. 3.

Fig. 4 shows damping of the inter-area mode when integrator gains of UPFC control system, K_{IP} and K_{IQ}, are changed independently with K_{PP} and K_{PQ} being zero. In this case, the supplementary damping control is not considered. Since proportional gains are held zero, the effect of the integrator gain on the damping of the inter-area mode is prominent. The figure shows that the improvement of damping is far more sensitive to the K_{IP}-a gain related to the V_P-when K_{IQ} has a low value. As the level of gains increases, the K_{IQ} becomes more significant. So it can be concluded that increasing both gains at the same time beyond some level is important for better damping. Setting K_{IP} and K_{IQ} as 0.5 gives damping of about 3%. Further damping enhancement can be accomplished by adjusting the proportional gain or adding a supplementary damping signal. This paper discusses a supplementary damping controller, (31), modulating the real power flow of the line from a locally measurable quantity in order to get additional damping.

D. Damping Controller Design

A lead-lag type regulator is considered as a damping controller. As a supplementary input signal, the difference between the real power flow of the line through UPFC and the P_{REF} (reference input of UPFC in Fig. 3) is considered as in [7]. As proposed in [15], angular difference of synthesized remote voltages can also be considered as a good input signal

$$V_{SUP} = K\frac{sT_W}{1+sT_W}\frac{1+sT_1}{1+sT_2}\Delta P_{\mathrm{line}}. \tag{31}$$

Fig. 5 shows the loci of inter-area mode with increasing gain, K, for various phase lead angles of the damping controller. The wash-out time constant is 5 s. Each controller constant is computed from the phase lead angle based on the formula used in [16]. It can be concluded from the figure that K should be negative or an additional 180° phase lead is needed with a positive K. The residue analysis shows that the inter-area mode is nearly in phase with the supplementary input, that is, V_P. So in order to increase damping of the inter-area mode, the negative feedback or phase lead about 180° would be desirable. Compared with increasing the proportional gain of the PI-controller, the damping control decreases the possibility of interaction of the UPFC with other power system phenomena such as torsional oscillations.

TABLE II
DAMPING OF INTER-AREA MODE FOR EACH CASE

Operating Point		Stiff	Median	Weak
W/O Damping Control	Case ID	I	II	III
	Damping(%)	5.81	3.24	- 0.353
With Damping Control	Case ID	IV	V	VI
	Damping(%)	29.1	19.6	11.4

Fig. 5 shows that as the phase lead angle of the damping controller increases, the frequency of the mode decreases excessively. So a phase lead angle of 15° seems to be a good initial setting. With a phase lead angle of 15°, K is set to be -0.09, which gives damping of the inter-area mode approximately 20%. With the damping control, two local modes of each area are nearly unaffected, which shows desirable characteristics of the damping controller.

Table II shows the damping of inter-area mode for six cases under consideration. For all cases, K_{IP} and K_{IQ} of the UPFC control system are set to be 0.5. Comparing Table I and Cases I-III of Table II shows that in the median and stiff system the damping of the inter-area mode is improved by installing UPFC, but in the weak system, the UPFC makes the system unstable. So the UPFC control system is vulnerable to operating point change. Cases IV-VI represents the case when the UPFC control system is equipped with a damping controller.

Fig. 6 shows the behavior of inter-area modes for each case more clearly. Dots indicate the inter-area mode for each operating point without a UPFC. Cases I-III indicates that the more the integrator gain is increased, the more the system becomes stable with the more damping. But the system is not robust against operating condition change. Fig. 6 also shows that increasing the integrator gain increases the frequency of the oscillation more than damping. Increasing gain also causes the controller to become more susceptible to saturation, which a nonwindup limit can resolve. Time domain simulation reveals that the performance of the control system deteriorates without

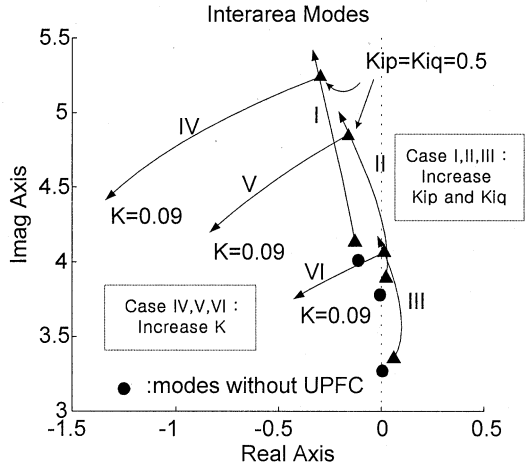

Fig. 6. Loci of inter-area mode for each cases.

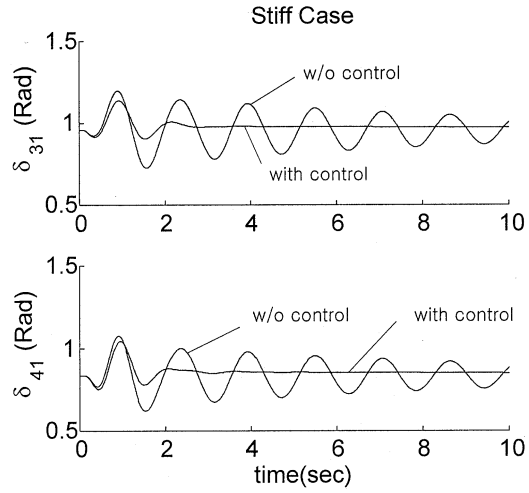

Fig. 7. Inter-area oscillations with and without damping control (Stiff system).

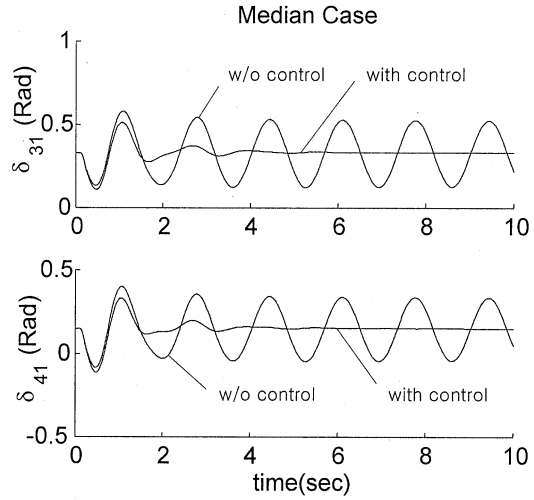

Fig. 8. Inter-area oscillations with and without damping control (Median system).

a nonwindup limit. Time domain simulations show that the transient line power flow saturates the integrator, which again dominate over the damping signal.

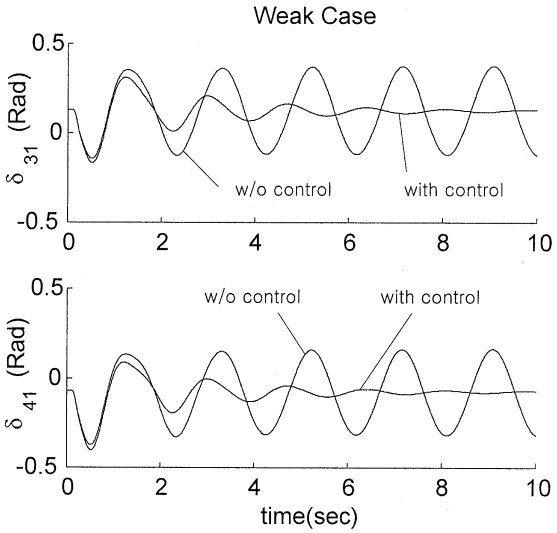

Fig. 9. Inter-area oscillations with and without damping control (Weak system).

Cases IV–VI indicates the case when a supplementary damping controller is added. Table II shows that the damping is greatly improved for all cases. Moreover, Fig. 6 shows that increasing gain mainly improves damping rather than frequency. The damping control is also robust against operating point change and the effect of damping is nearly uniform for each case.

E. Time Domain Simulations

Time domain simulations are performed for each system with and without damping control for a three-phase six-cycle fault applied to the load bus of area 1. The limit of series injected voltage is assumed to be 0.05 pu for both V_P and V_Q. A nonwindup limit of ± 0.1 is imposed on each integrator. Figs. 7–9 show the rotor angle oscillations between areas, which show that the oscillations are settled down after about 2–4 s.

Fig. 10 shows the case of operating point change from the median to weak case with a removal of a tie-line. The steady-state power flow through the tie-line does not change, but the transient power flow changes due to the constant impedance characteristics of the loads. Most of loads with constant power characteristics even have constant impedance characteristics at transient. Thus, the power flow change affects the input to the controller, which makes the damping controller saturate. Since the damping controller is tuned to the frequency range of the oscillations modes, it gradually filters out the offset component of the input signal and the oscillations are effectively damped out.

Fig. 11 shows the series injected voltage for cases III and VI. The damping controller prevents the UPFC from oscillating excessively. Fig. 12 shows the number of iterations at each step in time domain simulations. The proposed algorithm uses the converged value at the previous step as a starting point of the next step iteration. Simulation results show that the numbers of iterations are nearly constant except at a point where disturbance occurs. In Fig. 12, there are two jumps in the number of iterations. One is a point the fault occurs and

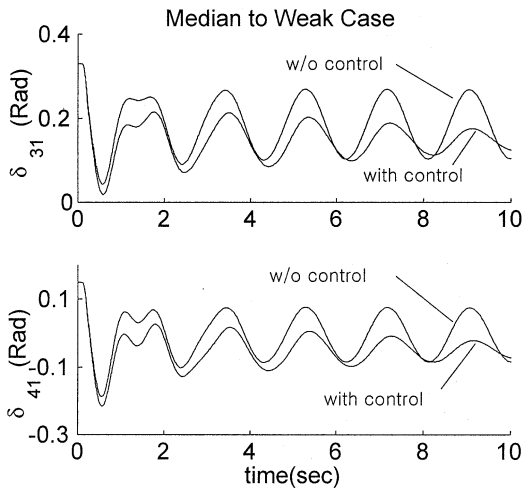

Fig. 10. Inter-area oscillations with operating point change (from Median to Weak).

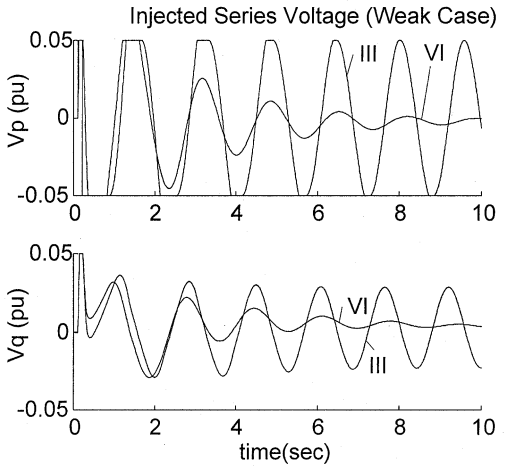

Fig. 11. Series injected voltage by UPFC with and without damping control (Weak system).

another is a point the fault is cleared. After about 1 s, the number of iterations is settled down to two iterations. The error tolerance for each step is set as $1e^{-9}$. The results show the fast convergence characteristics of the proposed algorithm.

The point that a damping signal is added is an important point of consideration. The damping signal can also be added to another point such as P_{REF} point in Fig. 3. However, if the damping signal loop contains an integrator, the transient performance of the damping controller becomes worse, which becomes evident from time simulations.

VI. Conclusions

This paper presents a Newton-type current injection model of the UPFC for studying low-frequency oscillations of a power system installed with a UPFC. Applicability of the proposed model to the damping control design and simulations are examined by studying the characteristics of a damping controller for inter-area oscillations of a sample power system with the proposed model both in the time and frequency domains.

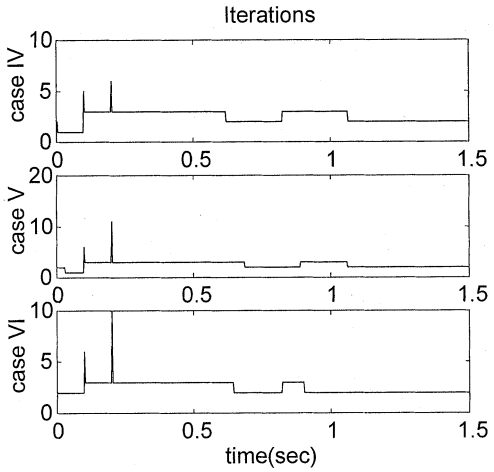

Fig. 12. Number of iterations for each step for cases IV, V, and VI.

The results show that the model is efficient for studying the dynamics of UPFC and designing damping controller.

Appendix

A. Elements of $\mathbf{J}^u$

Let $y_S = 1/x_S$, where x_S is series inverter transformer impedance, and define Y_S to be $Y_S = y_S(V_S/V_1^u)$, then the elements of $\mathbf{J}^u$ are as follows.

1) Expressions of $\mathbf{I}_P$

$$I_{PR} = -Y_S[V_2^u \sin(\theta_S - \theta_2^u) - V_1^u \sin(\theta_s - \theta_1^u)]\cos\theta_1^u \quad \text{(A1)}$$

$$I_{PI} = -Y_S[V_2^u \sin(\theta_S - \theta_2^u) - V_1^u \sin(\theta_s - \theta_1^u)]\sin\theta_1^u. \quad \text{(A2)}$$

2) Expressions of $\mathbf{I}_S$

$$I_{SR} = y_S V_S \sin(\theta_S + \theta_1^u) \quad \text{(A3)}$$

$$I_{SI} = -y_S V_S \cos(\theta_S + \theta_1^u). \quad \text{(A4)}$$

3) Elements of $\mathbf{J}^u$

$$\frac{\partial F_{R1}^u}{\partial V_1^u} = Y_S\left(\frac{V_2^u}{V_1^u}\right)\cos(\theta_S - \theta_2^u)\cos\theta_1^u - Y_{1,1}^u \cos(\theta_1^u + \phi_{1,1}^u) \quad \text{(A5)}$$

$$\frac{\partial F_{R1}^u}{\partial V_2^u} = -Y_S \sin(\theta_S - \theta_2^u)\cos\theta_1^u - Y_{1,2}^u \cos(\theta_2^u + \phi_{1,2}^u) \quad \text{(A6)}$$

$$\frac{\partial F_{R1}^u}{\partial \theta_1^u} = -Y_S[V_1^u \cos(\theta_S - \theta_1^u)\cos\theta_1^u + I_{PI}] + I_{SI} + Y_{1,1}^u V_1^u \cos(\theta_1^u + \phi_{1,1}^u) \quad \text{(A7)}$$

$$\frac{\partial F_{R1}^u}{\partial \theta_2^u} = Y_S V_2^u \cos(\theta_S - \theta_2^u)\cos\theta_1^u + Y_{1,2}^u V_2^u \sin(\theta_2^u + \phi_{1,2}^u) \quad \text{(A8)}$$

$$\frac{\partial F_{R2}^u}{\partial V_1^u} = -Y_{2,1}^u \cos(\theta_1^u + \phi_{2,1}^u) \quad \text{(A9)}$$

$$\frac{\partial F_{R2}^u}{\partial V_2^u} = -Y_{2,2}^u \cos(\theta_2^u + \phi_{2,2}^u) \quad \text{(A10)}$$

$$\frac{\partial F^u_{R2}}{\partial \theta^u_1} = Y_S V_2 \cos(\theta_S - \theta^u_1) + Y^u_{2,1} V^u_1 \sin(\theta^u_1 + \phi^u_{2,1}) \quad \text{(A11)}$$

$$\frac{\partial F^u_{R2}}{\partial \theta^u_2} = Y^u_{2,2} V^u_2 \sin(\theta^u_2 + \phi^u_{2,2}) \quad \text{(A12)}$$

$$\frac{\partial F^u_{I1}}{\partial V^u_1} = Y_S \left(\frac{V^u_2}{V^u_1}\right) \sin(\theta_S - \theta^u_2) \sin\theta^u_1 - Y^u_{1,1} \sin(\theta^u_1 + \phi^u_{1,1}) \quad \text{(A13)}$$

$$\frac{\partial F^u_{I1}}{\partial V^u_2} = -Y_S \sin(\theta_S - \theta^u_2) \sin\theta^u_1 - Y^u_{1,2} \sin(\theta^u_2 + \phi^u_{1,2}) \quad \text{(A14)}$$

$$\frac{\partial F^u_{I1}}{\partial \theta^u_1} = -Y_S [V^u_1 \cos(\theta_S - \theta^u_1) \sin\theta^u_1 - I_{PR}] - I_{SR} - Y^u_{1,1} V^u_1 \sin(\theta^u_1 + \phi^u_{1,1}) \quad \text{(A15)}$$

$$\frac{\partial F^u_{I1}}{\partial \theta^u_2} = Y_S V^u_2 \cos(\theta_S - \theta^u_2) \sin\theta^u_1 - Y^u_{1,2} V^u_2 \cos(\theta^u_2 + \phi^u_{1,2}) \quad \text{(A16)}$$

$$\frac{\partial F^u_{I2}}{\partial V^u_1} = -Y^u_{2,1} \sin(\theta^u_1 + \phi^u_{2,1}) \quad \text{(A17)}$$

$$\frac{\partial F^u_{I2}}{\partial V^u_2} = -Y^u_{2,2} \sin(\theta^u_2 + \phi^u_{2,2}) \quad \text{(A18)}$$

$$\frac{\partial F^u_{I2}}{\partial \theta^u_1} = y_S V_S \sin(\theta_S - \theta^u_1) - Y^u_{2,1} V^u_1 \cos(\theta^u_1 + \phi^u_{2,1}) \quad \text{(A19)}$$

$$\frac{\partial F^u_{I2}}{\partial \theta^u_2} = -Y^u_{2,2} V^u_2 \cos(\theta^u_2 + \phi^u_{2,2}). \quad \text{(A20)}$$

B. System Parameters

Each step-up transformer has an impedance of $j0.15$ pu on 900 MVA and 20/230 kV base. The transmission system nominal voltage is 230 kV. The line lengths are shown in Fig. 2. The parameters of the lines in pu on 100 MVA, 230 kV base are $r = 0.0001$ pu/km, $x_L = 0.001$ pu/km, $b_C = 0.001\,75$ pu/km.

Each generator has a rating of 900 MVA and 20 kV and the parameters in pu are as follows: $H = 58.5(G_1, G_2)$, $55.58(G_3, G_4)$, $D = 0$, $T'_{do} = 8.0$, $T'_{qo} = 0.4$, $X_d = 0.2$, $X'_d = 0.033$, $X_q = 0.18$, $X'_q = 0.033$.

The limit of the UPFC for damping control is assumed to be ± 0.05 pu each for the V_P and V_Q around the operating point. The shunt converter just provides the real power needed by the series inverter. Their limits are far below its steady-state capability in order not to make the system unstable due to the UPFC's action. It is assumed that the steady-state control limit is 600 MVA with injected voltage 1.2 pu, current 5 pu, shunt converter current 6 pu on 100 MVA, 230 kV base. The steady-state ratings, however, does not matter in this paper because this paper deals with small-signal problems that are associated with low-frequency oscillations.

REFERENCES

[1] "CIGRE an IEEE Working Groups on FACTS, FACTS Overview," IEEE Power Eng. Soc., 95TP108, 1995.

[2] L. Gyugyi, G. D. Schauder, S. L. Williams, T. R. Rietman, D. R. Torgerson, and A. Edris, "The unified power flow controller: A new approach to power transmission control," *IEEE Trans. Power Delivery*, vol. 10, pp. 1085–1097, Apr. 1995.

[3] A. Nabavi-Niaki and M. R. Iravani, "Steady-State and dynamic models of unified power flow controller (UPFC) for power system studies," *IEEE Trans. Power Syst.*, vol. 11, pp. 1937–1943, Nov. 1996.

[4] M. Noroozian, L. Angquist, M. Ghandhari, and G. Andersson, "Improving power system dynamics by series-connected FACTS devices," *IEEE Trans. Power Delivery*, vol. 12, pp. 1635–1641, Oct. 1997.

[5] K. R. Padiyar and K. U. Rao, "Modeling and control of unified power flow controller for transient stability," *Int. J. Electr. Power Energy Syst.*, vol. 21, no. 1, pp. 1–11, 1999.

[6] S. Arabi, P. Kundur, and R. Adapa, "Innovative techniques in modeling UPFC for power system analysis," *IEEE Trans. Power Syst.*, vol. 15, pp. 336–341, Feb. 2000.

[7] Z. Huang, Y. Ni, C. M. Shen, F. F. Wu, S. Chen, and B. Zhang, "Application of unified power flow controller in interconnected power systems—Modeling, interface, control strategy and case study," *IEEE Trans. Power Syst.*, vol. 15, pp. 817–824, May 2000.

[8] H. F. Wang, "A unified model for the analysis of FACTS devices in damping power system oscillations—Part III: Unified power flow controller," *IEEE Trans. Power Delivery*, vol. 15, pp. 978–983, July 2000.

[9] S. Bruno, E. De Tugile, M. L. La Scala, and P. Scrpellini, "Dynamic security corrective control by UPFC's," *IEEE Trans. Power Syst.*, vol. 16, pp. 490–497, Aug. 2001.

[10] H. Fujita, Y. Watanabe, and H. Akagi, "Transient analysis of a unified power flow controller and its application to design of the DC-link capacitor," *IEEE Trans. Power Electron.*, vol. 16, pp. 735–740, Sept. 2001.

[11] P. Kundur, *Power System Stability and Control*. New York: McGraw-Hill, 1994.

[12] K. M. Son and J. K. Park, "On the robust LQG control of TCSC for damping power system oscillations," *IEEE Trans. Power Syst.*, vol. 15, pp. 1306–1312, Nov. 2000.

[13] G. N. Taranto and J. H. Chow, "A robust frequency domain optimization technique for tuning series compensation damping controllers," *IEEE Trans. Power Syst.*, vol. 10, pp. 1219–1225, Aug. 1995.

[14] J. Bian, D. G. Ramey, R. J. Nelson, and A. Edris, "A study of equipment sizes and constraints for a unified power flow controller," *IEEE Trans. Power Delivery*, vol. 12, pp. 1385–1391, July 1997.

[15] E. V. Larsen, J. J. Sanchez-Gasca, and J. H. Chow, "Concepts for design of FACTS controllers to damp power swings," *IEEE Trans. Power Syst.*, vol. 10, pp. 948–956, May 1995.

[16] N. Yang, Q. Liu, and J. D. McCalley, "TCSC controller design for damping interarea oscillations," *IEEE Trans. Power Syst.*, vol. 13, pp. 1304–1310, Nov. 1998.

Kwang M. Son (M'94) received the B.S., M.S., and Ph.D. degrees in electrical engineering from Seoul National University, Seoul, Korea in 1989, 1991, and 1996, respectively.

He is currently an Assistant Professor with Dong-Eui University, Pusan, Korea. He was an Honorary Fellow at the University of Wisconsin-Madison in 2001. His research interests include flexible ac transmission systems (FACTS) and distributed resources.

Robert H. Lasseter (M'74–SM'89–F'92) received the Ph.D. degree in physics from the University of Pennsylvania, Philadelphia, in 1971.

He was a Consultant Engineer with the General Electric Company until 1980, when he joined the University of Wisconsin-Madison. His main research interests are microgrids and the application of power electronics to utility systems including hardware, methods of analysis, and simulation.